

## REPORT DOCUMENTATION PAGE

1a. REPORT SECURITY CLASSIFICATION Unclassified		1b. RESTRICTIVE MARKINGS	
2a. SECURITY CLASSIFICATION AUTHORITY		3. DISTRIBUTION/AVAILABILITY OF REPORT This document has been approved for public release and sale; it's distribution is unlimited	
2b. DECLASSIFICATION/DOWNGRADING SCHEDULE			
4. PERFORMING ORGANIZATION REPORT NUMBER(S)  Technical Report #8		5. MONITORING ORGANIZATION REPORT NUMBER(S)  4133046	
6a. NAME OF PERFORMING ORGANIZATION  University of Minnesota	6b. OFFICE SYMBOL (If applicable)  ONR	7a. NAME OF MONITORING ORGANIZATION  Office of Naval Research	
6c. ADDRESS (City, State, and ZIP Code) Dept. of Chemical Eng. & Materials Science University of Minnesota Minneapolis, MN 55455		7b. ADDRESS (City, State, and ZIP Code) 800 Quincy Street North Arlington, VA 22217-5000	
8a. NAME OF FUNDING/SPONSORING ORGANIZATION  Office of Naval Research	8b. OFFICE SYMBOL (If applicable)  ONR	9. PROCUREMENT INSTRUMENT IDENTIFICATION NUMBER  Grant N00014-93-1-0563	
8c. ADDRESS (City, State, and ZIP Code) 800 North Quincy Street Arlington, VA 22217-5000		10. SOURCE OF FUNDING NUMBERS  PROGRAM ELEMENT NO.      PROJECT NO.      TASK NO.      WORK UNIT ACCESSION NO.	

11. TITLE (Include Security Classification)  
Molecular Nanoclusters as Precursors to Conductive Thin Films and Crystals

12. PERSONAL AUTHOR(S)  
Andrew C. Hillier, Joachim Hossick Schott, and Michael D. Ward

13a. TYPE OF REPORT Technical	13b. TIME COVERED FROM 5/1/94 TO 6/30/95	14. DATE OF REPORT (Year, Month, Day) 1995 January 20	15. PAGE COUNT 16
----------------------------------	---	--	----------------------

## 16. SUPPLEMENTARY NOTATION

17. COSATI CODES			18. SUBJECT TERMS (Continue on reverse if necessary and identify by block number)
FIELD	GROUP	SUB-GROUP	
			Organic Conductor/Atomic Force Microscopy/Scanning Electron Microscopy/Nucleation

## 19. ABSTRACT (Continue on reverse if necessary and identify by block number)

• Research News: The fabrication of electrically conductive organic thin films and crystals is of both fundamental and technological interest. However, the mechanisms that control crystal structure and morphology during crystallization are not yet completely understood. In order to address these issues, we have employed scanning tunneling and atomic force microscopies to view the formation of molecular conductors on single crystal substrates. We have observed that these materials form ordered molecular nanoclusters, in which at least one dimension has molecular length scale. These nanoclusters evolve into thin films, and eventually, bulk crystals. The role of interactions between the substrate and organic overlayers, as well as the influence of intermolecular interactions within the molecular clusters, has been revealed.

DTIC QUALITY INSPECTED 3

20. DISTRIBUTION/AVAILABILITY OF ABSTRACT <input checked="" type="checkbox"/> UNCLASSIFIED/UNLIMITED <input type="checkbox"/> SAME AS RPT. <input type="checkbox"/> DTIC USERS	21. ABSTRACT SECURITY CLASSIFICATION Unclassified
22a. NAME OF RESPONSIBLE INDIVIDUAL Robert Nowak	22b. TELEPHONE (Include Area Code) X(612) 703-696-4409    22c. OFFICE SYMBOL ONR Code 1113

OFFICE OF NAVAL RESEARCH

GRANT # N00014-93-1-0563

R&T Code 4133046

Technical Report # 8

Accession For	
NTIS	CRA&I
DTIC	TAB
Unannounced	
Justification _____	
By _____	
Distribution / _____	
Availability Codes	
Dist	Avail and/or Special
A-1	

"Molecular Nanoclusters as Precursors to Conductive Thin  
Films and Crystals"

19950130 007

by

Andrew C. Hillier, Joachim Hossick Schott, and Michael D. Ward

Prepared for Publication by Invitation

in

Advanced Materials

Department of Chemical Engineering and Materials Science  
University of Minnesota  
Amundson Hall  
421 Washington Ave. SE  
Minneapolis, MN 55455

January 20, 1995

Reproduction in whole, or in part, is permitted for any purpose of the United States Government.

This document has been approved for public release and sale, its distribution is unlimited.

# **Molecular Nanoclusters as Precursors to Conductive Thin Films and Crystals**

Andrew C. Hillier, Joachim Hossick Schott and Michael D. Ward\*

*Department of Chemical Engineering and Materials Science  
University of Minnesota, Amundson Hall  
421 Washington Ave. SE, Minneapolis, MN 55455*

## **Table of Contents Abstract**

**Research News: The fabrication of electrically conductive organic thin films and crystals** is of both fundamental and technological interest. However, the mechanisms that control crystal structure and morphology during crystallization are not yet completely understood. In order to address these issues, we have employed scanning tunneling and atomic force microscopies to view the formation of molecular conductors on single crystal substrates. We have observed that these materials form ordered molecular nanoclusters, in which at least one dimension has molecular length scale. These nanoclusters evolve into thin films, and eventually, bulk crystals. The role of interfacial interactions between the substrate and organic overlayers, as well as the influence of intermolecular interactions within the molecular clusters, has been revealed.

## **1. Introduction**

Considerable effort has been expended on the design and synthesis of crystalline, electrically conductive organic charge-transfer salts. Interest in these materials stems from the potential to employ molecular-level "crystal engineering" strategies to rationally manipulate crystal packing and, consequently, influence bulk physical and electronic properties. While these materials have limited potential in applications requiring crystals of macroscopic dimensions, they are attractive candidates for "nanostructures," in which at least one physical dimension has molecular length scale. In these structures, physical and electronic properties will depend upon the characteristics of the molecular constituents. Typical nanostructures may include nanometer-scale wires, for which anisotropic low-dimensional conductors are particularly well-suited as they tend to form needle-like crystals, or organic thin films capable of forming heterostructures with molecular-scale dimensions. In order to create nanostructures based on molecular conductors, the self-assembly, nucleation, and crystal growth processes that are responsible for their formation must be understood and controlled. The influence of substrates is of particular interest, especially with respect to growth orientation, morphology, polymorph selection, and stability. Control of these characteristics demands attention to epitaxial (or quasiepitaxial) interactions at the growth interface<sup>1,2,3</sup> and to intermolecular bonding within the crystalline nanostructure. Below we highlight recent examples from our laboratories in which the formation of organic "nanoclusters" on single crystal substrates illustrates the influence of these factors.

## **2. Growth of (TTF)(TCNQ) nanoclusters**

One of the best known low-dimensional organic conductors is the charge-transfer salt (TTF)(TCNQ), which was the first "organic metal" discovered.<sup>4</sup> The bulk crystal structure of this material reveals segregated stacks of TTF cations and TCNQ anions, with the stacks oriented along the crystallographic *b* axis. (TTF)(TCNQ) forms needle-shaped crystals when crystallized from solutions containing the molecular constituents or when grown by sublimation (the salt has an appreciable vapor pressure). The needle axis of the macroscopic crystal corresponds to the crystallographic *b* axis, which is the stacking axis.

Brief exposure of Au(111) surfaces to (TTF)(TCNQ) vapor (TTF = tetrathiafulvalene; TCNQ = tetracyanoquinodimethane) under ambient conditions resulted in adsorption with the formation of irregularly shaped, two-dimensional clusters ( $\approx 10^4$  nm $^2$ ).<sup>5</sup> These clusters were readily observed by STM (Fig. 1A, B) and exhibited an average thickness of 1.5 Å.

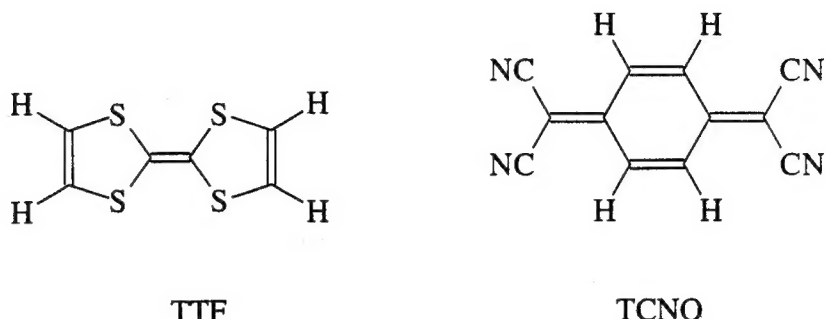


[Figure 1]

The lattice constants determined from the periodicity of tunneling current contrast of these nanoclusters (denoted as Type I in reference 5)<sup>6</sup> at high resolution were  $b_1 = 11.0 \pm 1$  Å,  $b_2 = 16.5 \pm 1$  Å, and  $\beta = 104^\circ \pm 1^\circ$ , similar to those of the *ac* plane of the bulk crystal (monoclinic P2<sub>1</sub>/c,  $a = 12.298$  Å,  $b = 3.819$  Å,  $c = 18.468$  Å,  $\beta = 104.46^\circ$ ). This observation, combined with the measured 1.5 Å thickness, was consistent with an overlayer in which the TTF and TCNQ planes are parallel (or nearly so) with the Au (111) substrate (Fig. 1C). The observation of an apparent monolayer height which was less than the 3.8 Å molecular thickness of TTF and TCNQ can be attributed to the lower tunneling probability of the organic overlayer. The STM data also displayed large scale corrugations in the tunneling current with typical periodicities of 150 - 200 Å (Fig. 1A). The source of these corrugations was attributed, based on modeling studies, to Moiré patterns that resulted from the superposition of (TTF)(TCNQ) overlayer wavefunctions with those of the Au(111) surface. The (TTF)(TCNQ) nanoclusters displayed Moiré patterns with varying periodicity and regularity, indicating that the nanoclusters did not exhibit preferred azimuthal orientations with respect to the Au(111) substrate.

Exposure of the Au(111) surface to (TTF)(TCNQ) vapor for longer times resulted in clusters having thicknesses corresponding to two or three molecular layers (Figure 2A). In contrast

to the monolayer clusters, these regions exhibit a high resolution ribbon motif with an interribbon distance of  $5 \pm 1$  Å, approximately equivalent to  $a/2$ . This behavior can be explained by considering the molecular overlap of TTF and TCNQ molecules between  $ac$  layers along the stacking axis, as deduced from the single crystal x-ray structure. Within the segregated stacks, TTF and TCNQ molecules exhibit "ring-over-bond" overlaps in which adjacent molecules are slipped with respect to each other along their long molecular axes by an amount approximately equal to  $c/4$ . This configuration leads to a spatial distribution of the electronic states associated with TTF and TCNQ molecules in layer  $n+1$  that is shifted by  $c/4$  with respect to molecules in layer  $n$ , when viewed normal to the molecular planes. Indeed, the experimentally observed STM ribbon motif in Fig. 2A was replicated by adding the numerical contrast values from high resolution images of two  $ac$  layers, in which one of the layers is translated by  $c/4$  (Figure 2C). The enhanced intermolecular overlap between TTF and TCNQ molecules results in greater continuity of the density of states (DOS) along the  $c$  direction, but with negligible change in the interribbon overlap and DOS along the  $a$  axis. This pronounced anisotropy of the DOS associated with the  $c$ -oriented chains is tantamount to an array of "molecular wires."

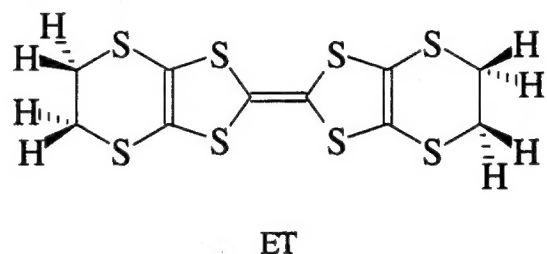
The evolution from the monolayer to the multilayer clusters reveals the sequence of molecular events leading to the formation of bulk crystals of (TTF)(TCNQ). Notably, prolonged exposure of the Au(111) surface to (TTF)(TCNQ) vapor resulted in the formation of needles of (TTF)(TCNQ) whose long axis was perpendicular to the Au substrate surface. Since the needle axis is coincident with the stacking  $b$ -axis, the orientation of the Type I nanoclusters governed the orientation of the bulk crystals.

### [Figure 2]

## 3. Molecular Films of $\beta$ -(ET)<sub>2</sub>I<sub>3</sub>: Electrochemical Deposition

An alternative approach to vapor phase fabrication of organic thin films and nanostructures is electrochemical crystallization. Electrococrystallization is commonly employed for the synthesis of organic charge-transfer salts. The advantages of this technique over vapor phase deposition include precise control of the concentration of solute at the interface and the ability to fabricate thin films and nanostructures on substrates with unusual geometries.

However, previous reports have indicated that electrocrystallization of bulk crystals of the organic conductor  $(ET)_2I_3$  ( $ET =$  bis(ethylenedithiolo)tetrathiafulvalene) occurs with the simultaneous formation of several phases, with  $\alpha$  and  $\beta$  phases predominating.<sup>7</sup> Notably, electrocrystallization of  $(ET)_2I_3$  at untreated graphite electrodes was shown to favor the formation of  $\beta$ - $(ET)_2I_3$ ,<sup>8</sup> whereas electrochemically oxidized graphite electrodes afforded  $\alpha$ - $(ET)_2I_3$ . This behavior suggested that interfacial interactions between  $\beta$ - $(ET)_2I_3$  and graphite during nucleation may be a significant factor in determining phase selectivity. We therefore employed in-situ atomic force microscopy (AFM) to examine the formation of  $(ET)_2I_3$  charge-transfer salts.<sup>9</sup>



When an anodic potential of  $E_{app} \approx 650$  mV (vs Ag/AgCl), sufficient to oxidize ET, was applied to a freshly cleaved HOPG electrode in acetonitrile solutions containing ET and  $I_3^-$ , AFM revealed the formation of  $(ET)_2I_3$  in two distinct monolayer orientations, which we identify as Type IIa and Type IIb.<sup>10</sup> The Type IIa monolayer formed by aggregation of two-dimensional clusters, which emerged from discrete locations on the HOPG terraces and exhibited a preferred faceting of  $10^\circ \pm n60^\circ$  with respect to the graphite lattice vectors (Fig. 3A).<sup>11</sup> The height of these clusters was 15.5 Å (Fig. 3B), indicating that the long axes of the ET molecules were nearly perpendicular to the graphite substrate. Grain boundaries, which formed between individual clusters, rapidly annealed to form an apparently defect-free (by AFM) monolayer. The monolayer was stable indefinitely at  $E > 650$  mV, and could be formed and removed repeatedly upon potential cycling.

High resolution AFM imaging of the Type IIa  $(ET)_2I_3$  monolayer (Fig. 3C) revealed a structure resembling that observed for the *ab* face of single crystal  $\beta$ - $(ET)_2I_3$ . The real-space AFM data exhibited a strong periodicity with lattice parameters of  $b_1 = 12.0 (\pm 0.8)$  Å,  $b_2 = 8.5$

( $\pm 0.8$ ) Å, and  $\gamma = 108^\circ (\pm 3)$ . This lattice corresponded to the smallest reciprocal cell observed in Fourier analysis of the data. Although  $\mathbf{b}_1$  was twice the expected crystallographic value ( $P\bar{1}$ ,  $a = 6.6$  Å ( $\approx 1/2 \mathbf{b}_1$ ),  $b = 9.1$  Å ( $\approx \mathbf{b}_2$ ),  $c = 15.3$  Å and  $\gamma = 110^\circ$ ), Fourier analysis revealed a larger reciprocal cell corresponding to a unit cell with  $\mathbf{b}_3 = 6.0 (\pm 0.8)$  Å,  $\mathbf{b}_2 = 8.5 (\pm 0.8)$  Å, and  $\gamma = 108^\circ (\pm 3)$ , in near exact agreement with the crystallographic parameters of the *ab* plane (Fig. 3D). The assignment of a  $\beta$ -like monolayer structure was further corroborated by the 15.5 Å monolayer height, which is equivalent to the thickness of *ab* layers in bulk  $\beta$ -(ET)<sub>2</sub>I<sub>3</sub>. Recent experiments have confirmed the presence of a  $\beta$ -(ET)<sub>2</sub>I<sub>3</sub> monolayer (denoted Type IIb) whose structure and thickness are consistent with the short axis of ET lying perpendicular to the HOPG substrate. High resolution AFM images of this monolayer indicate a unit cell corresponding to the  $(\bar{1}10)$  face of  $\beta$ -(ET)<sub>2</sub>I<sub>3</sub>. Space does not permit us to elaborate on the nature or influence of this monolayer on crystal growth, but full details will be disclosed shortly.<sup>12</sup>

### [Figure 3]

The observed faceting of the Type IIa monolayer cluster at  $10^\circ \pm n60^\circ$  with respect to the graphite lattice vectors suggested the presence of a quasiepitaxial interaction between the  $\beta$ -(ET)<sub>2</sub>I<sub>3</sub> monolayer and HOPG. In order to determine the azimuthal relationship between the HOPG and monolayer lattices, the AFM tip was rastered over a small region of the monolayer at a higher force ( $F > 20$  nN) than that used for imaging. This resulted in mechanical removal of the monolayer, which allowed high resolution imaging of the HOPG substrate directly beneath the monolayer. This revealed an azimuthal orientation for the  $\beta$ -(ET)<sub>2</sub>I<sub>3</sub> overlayer corresponding to  $\mathbf{b}_1 = 4.9\mathbf{a}_1 + 1.1\mathbf{a}_2$  and  $\mathbf{b}_2 = 3.86(\mathbf{a}_2 - \mathbf{a}_1)$ , where  $\mathbf{a}_1$  and  $\mathbf{a}_2$  are the graphite lattice vectors (Fig. 3D). This was consistent with a coincident overlayer having a  $\beta$ -(ET)<sub>2</sub>I<sub>3</sub> supercell with dimensions  $\mathbf{b}_1 \times 3 \mathbf{b}_2$ . A geometrical analysis of the (001)  $\beta$ -(ET)<sub>2</sub>I<sub>3</sub>/HOPG interface indicated several orientations of commensurism including the observed orientation. In contrast, commensurism could not be found for the (001)  $\alpha$ -(ET)<sub>2</sub>I<sub>3</sub>/HOPG interface.

At applied potentials slightly exceeding 650 mV, microscopic single crystals emerged from the Type IIa monolayer at discrete locations on the HOPG substrate. AFM revealed that

the growth of these crystals occurred by a layering mechanism wherein *ab* layers emerged from a single screw dislocation and spread across the crystal surface. These microcrystals were identified as  $\beta$ -(ET)<sub>2</sub>I<sub>3</sub>, based upon AFM goniometry<sup>13</sup> and from high resolution imaging of the exposed crystal faces. The crystals were oriented with the (001) face parallel to the substrate, identical to the orientation of the monolayer. These observations indicated that the Type IIa monolayer led to the formation of macroscopic (001)-oriented  $\beta$ -(ET)<sub>2</sub>I<sub>3</sub> crystals on HOPG. That is, a quasiepitaxial interaction between the  $\beta$ -(ET)<sub>2</sub>I<sub>3</sub> overlayer and the basal plane of HOPG is responsible for the polymorph selectivity observed during electrocrystallization on ordered graphite substrates. In contrast, monolayer formation was not observed on electrochemically roughened HOPG. Rather, the exclusive crystallization of  $\alpha$ -(ET)<sub>2</sub>I<sub>3</sub> microcrystals was observed on this substrate (microcrystals of  $\alpha$ -(ET)<sub>2</sub>I<sub>3</sub> and  $\beta$ -(ET)<sub>2</sub>I<sub>3</sub> could be distinguished by high resolution AFM and their morphology).<sup>14</sup>

### 3. The Role of Epitaxy and Orientation in Nanocluster Morphology

Comparison of the molecular clusters comprising (TTF)(TCNQ) and  $\beta$ -(ET)<sub>2</sub>I<sub>3</sub> is interesting from the standpoint of the observed morphologies and orientations of these clusters. The absence of preferred azimuthal orientation for (TTF)(TCNQ) on Au(111) indicated a weak interfacial interaction, whereas distinct orientations were observed for  $\beta$ -(ET)<sub>2</sub>I<sub>3</sub> on graphite. The (TTF)(TCNQ) *ac* clusters were oriented so that the molecular planes were parallel to the Au(111) surface and the one-dimensional stacking axis was normal to the interface. Consequently, the strongest intermolecular interactions were normal to the growth interface (Fig. 4A). In contrast, the Type IIa  $\beta$ -(ET)<sub>2</sub>I<sub>3</sub> *ab* monolayer (Type IIa) was oriented with the long molecular axis of ET normal to the graphite surface, so that strong charge-transfer interactions along the stacking axis and S-S intermolecular interactions were within the layer and parallel to the growth interface. The Type IIb  $\beta$ -(ET)<sub>2</sub>I<sub>3</sub> monolayer was also oriented with the stacking axis parallel to the interface, but the S-S intermolecular interactions within the layer were absent (Fig. 4B). These factors conspire to influence the orientation and morphology of the monolayers and the emerging crystals. The area of the  $\beta$ -(ET)<sub>2</sub>I<sub>3</sub> monolayers was significantly larger than that of the (TTF)(TCNQ) nanoclusters. Furthermore, needles of (TTF)(TCNQ) grow normal to the substrate, whereas Type IIa  $\beta$ -(ET)<sub>2</sub>I<sub>3</sub> monolayers are two-dimensional and form large plate-like

crystals on the substrate. In the case of the Type IIb cluster, the absence of S-S interactions within the layer leads to rapid growth of the monolayers along one-dimension parallel to the substrate and the formation of needle-shaped crystals. These examples illustrate that the anisotropy and direction of intermolecular bonding with respect to the interface, as well as interfacial interactions, are important factors in controlling the growth of thin films and crystals of molecular conductors. The ability to prepare large highly ordered organic mono- and multilayers whose structure mimics that of an organic solid that has been demonstrated to exhibit metallic conductivity and superconductivity has interesting implications for the fabrication of electronic devices based on molecular components.

[Figure 4]

## References

---

- 1 (a) M. Mobus, N. Karl, T. Kobayashi, *J. Cryst. Growth* **1992**, *116*, 495. (b) L.K. Chau, C.D. England, S. Chen, N.R. Armstrong, *J. Phys. Chem.* **1993**, *97*, 2699.
- 2 Y.Z. Li, M. Chander, J.C. Patrin, J.H. Weaver, L.P.F. Chibante, R.E. Smalley, *Science* **1991**, *253*, 429.
- 3 P.E. Burrows, Y. Zhang, E.I. Haskal, S.R. Forrest, *Phys. Rev. Lett.* **1992**, *61*, 2417.
- 4 T.J. Kistenmacher, T.E. Philipps, D.O. Cowan, *Acta. Crystallogr.* **1973**, *B30*, 763.
- 5 J. Hossick-Schott, M.D. Ward, *J. Am. Chem. Soc.* **1994**, *116*, 6806.
- 6 In this and related publications, Type I clusters refer to those wherein the molecular stacking axis is perpendicular to the substrate surface. In contrast, Type II clusters are those having the molecular stacking axis parallel to the substrate.
- 7 R.P. Shibaeva, V.F. Kaminskii, E.B. Yagubskii, *Mol. Cryst. Liq. Cryst.* **1985**, *119*, 361.
- 8 H.H. Wang, L.K. Montgomery, C.A. Husting, B.A. Vogt, J.M. Williams, S.M. Budz, M.J. Lowry, K.D. Carlson, W.-K. Kwok, V. Mikheyev, *Chem. Mat.* **1989**, *1*, 484.
- 9 A.C. Hillier, J.B. Maxson, M.D. Ward, *Chem. Mater.* in press.
- 10 The Type IIa monolayer orientation was described in ref(9). Both Type IIa and Type IIb monolayers will be discussed in a forthcoming publication.
- 11 The graphite lattice directions are indicated by the observed step orientations, which generally cleave along the {1210} family of directions.
- 12 A.C. Hillier, J.B. Maxson, M.D. Ward, in preparation.
- 13 A.C. Hillier, M.D. Ward, *Science* **1994**, *263*, 1261.
- 14 Crystals of  $\beta$ -(ET)<sub>2</sub>I<sub>3</sub> exhibit a flat, distorted hexagonal morphology whereas  $\alpha$ -(ET)<sub>2</sub>I<sub>3</sub> crystal are rectangular plates. The large face in both phases corresponds to the (001) crystal face.

## Figure Captions

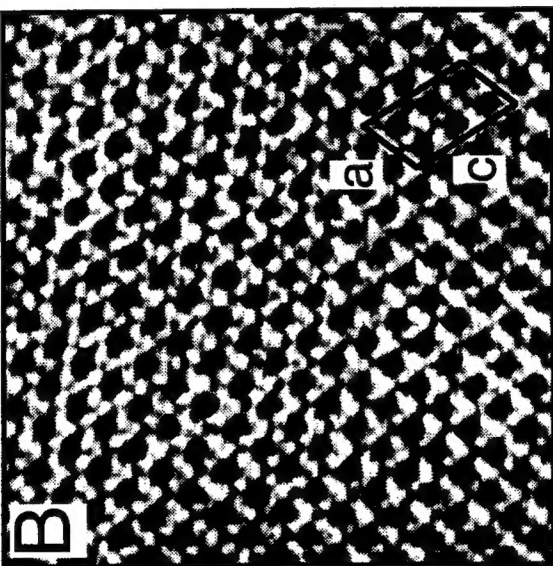
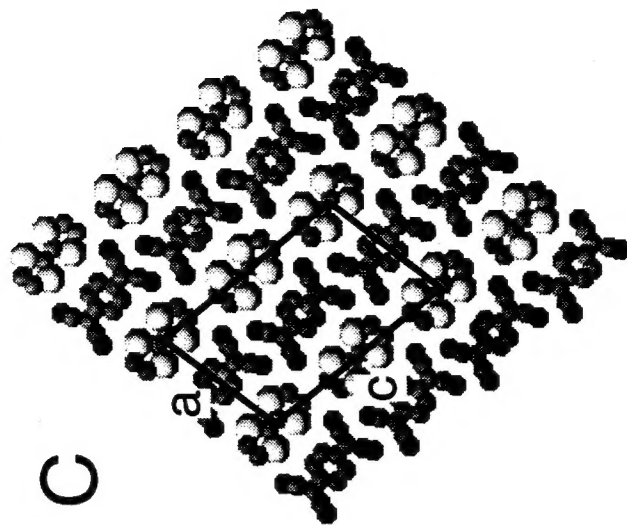
**Figure 1.** STM images of (TTF)(TCNQ) nanoclusters on the Au(111) surface: (A) Large area of a monolayer-thick nanocluster. The clusters exhibit large scale contrast patterns due to the convolution of the density of states of the organic monolayer and the gold substrate. (B) A magnified section of the STM data from (A), with the molecular motif of the (TTF)(TCNQ) *ac* plane obtained from the single crystal x-ray structure. The *ac* unit cell (C) is arranged in an azimuthal orientation in which the unit cell dimensions agree with the tunneling current contrast.

**Figure 2.** (A) STM image of a molecular *ac* multilayer, which exhibits tunneling current contrast associated with molecular ribbons along the crystallographic *c*-axis of (TTF)(TCNQ). (B) Computer generated superposition of two STM images from the same molecular *ac* monolayer obtained after a *c*/4 glide symmetry operation of one of the layers. (C) Molecular model of two superimposed *ac* monolayer sheets related by a *c*/4 translation, simulating the *c*/4 translation of the molecules in layer *n*+1 with respect to layer *n*. Note that each molecule in the upper layer overlaps only partially with the molecule in the layer beneath, resulting in imaging of segregated, electronically continuous TTF and TCNQ ribbons along the *c* axis. The distance between neighboring ribbons is *a*/2.

**Figure 3.** (A) In-situ AFM image acquired after 210 seconds of growth of an (ET)<sub>2</sub>I<sub>3</sub> monolayer in acetonitrile on a freshly cleaved HOPG electrode. The formation of the monolayer commenced after a potential step of 600 mV (vs Ag/AgCl). (B) A height profile analysis of the (ET)<sub>2</sub>I<sub>3</sub> monolayer and a neighboring graphite step is indicated. (C) In-situ high resolution AFM data (raw data) for the  $\beta$ -(ET)<sub>2</sub>I<sub>3</sub> monolayer. The real-space data exhibit a strong contrast periodicity of  $\mathbf{b}_1 = 12.0 (\pm 0.8)$  Å and  $\mathbf{b}_2 = 8.5$  Å ( $\pm 0.8$ ) with  $\gamma = 108^\circ$ . The unit cell of the monolayer, depicted by the black outline, compares favorably with the *ab* face of  $\beta$ -(ET)<sub>2</sub>I<sub>3</sub> depicted in (D), for which  $a = 6.6$  Å ( $\approx 1/2 \mathbf{b}_1$ ),  $b = 9.1$  Å ( $\approx \mathbf{b}_2$ ), and  $\gamma = 110^\circ$  by x-ray diffraction.

**Figure 4.** Schematic representation of the orientation and intermolecular bonding of (TTF)(TCNQ) and (ET)<sub>2</sub>I<sub>3</sub> molecular clusters and crystals. (A) In the case of (TTF)(TCNQ), the *ac* layer forms on the Au(111) surface with strong intermolecular  $\pi-\pi$  interactions ( $\phi^{\pi-\pi}$ )

oriented normal to the *ac* layer and the substrate surface. These characteristics lead to nanoclusters with small lateral dimensions and needles growing normal to the substrate. (B) Type IIa layers of  $\beta$ -(ET)<sub>2</sub>I<sub>3</sub> have strong intermolecular  $\pi$ - $\pi$  and S-S interactions ( $\phi^{\pi-\pi}$  and  $\phi^{S-S}$ ) oriented parallel to the substrate, leading to a large, morphologically stable, two-dimensional monolayer. Type IIb  $\beta$ -(ET)<sub>2</sub>I<sub>3</sub> monolayers also cover large regions of the substrate, but are more anisotropic as the S-S interactions ( $\phi^{S-S}$ ) within the layer are absent. The insets depict microscopic bulk crystals of each compound, which evolve from the nanoclusters.



2 nm

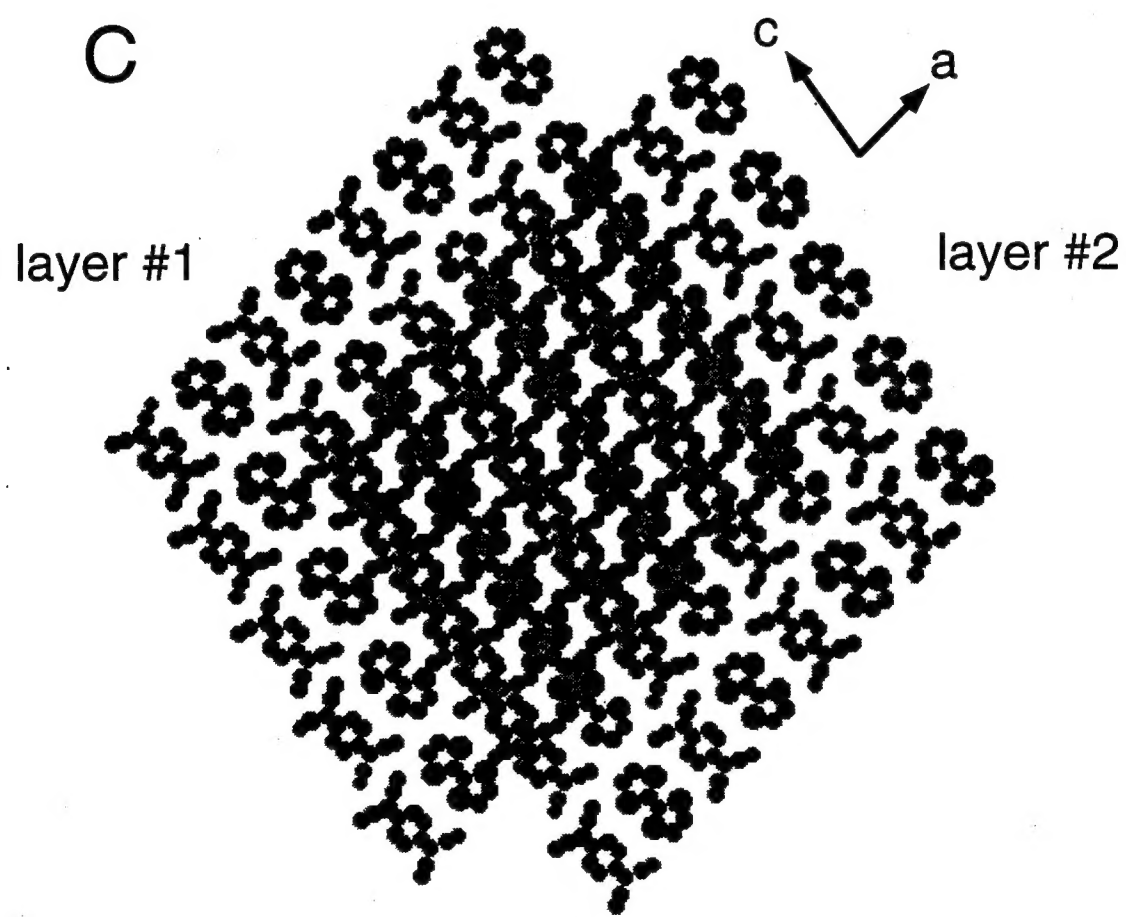
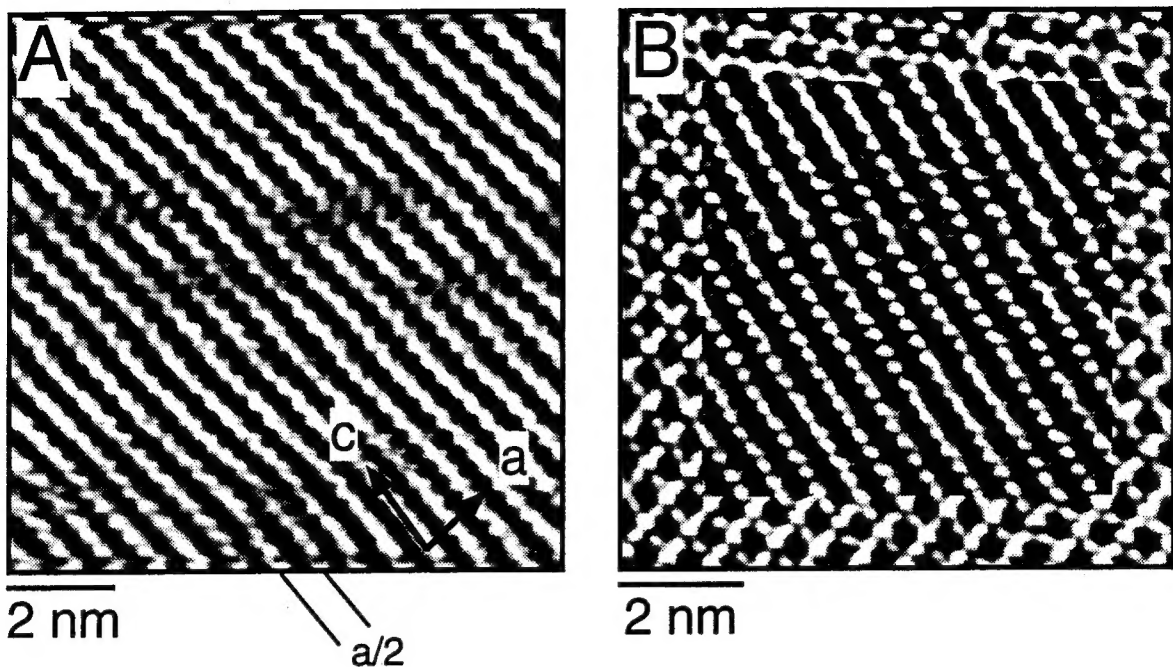


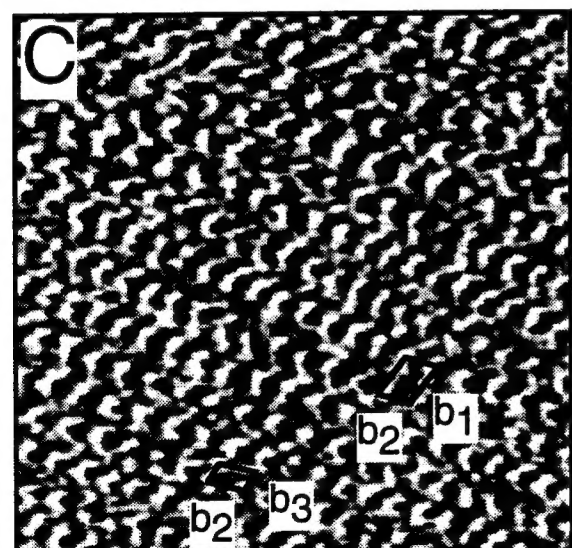
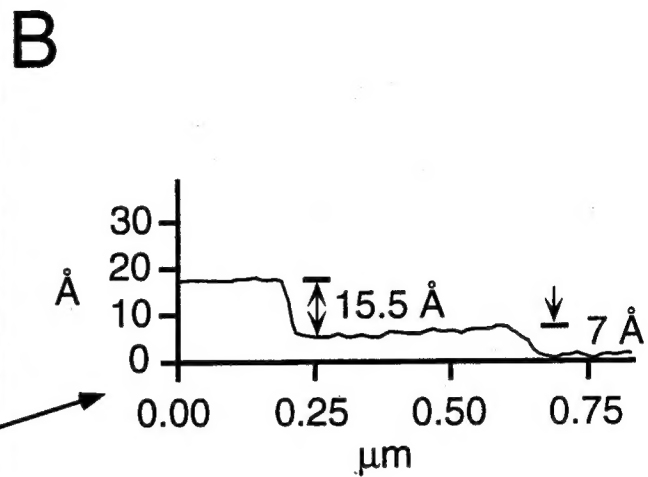
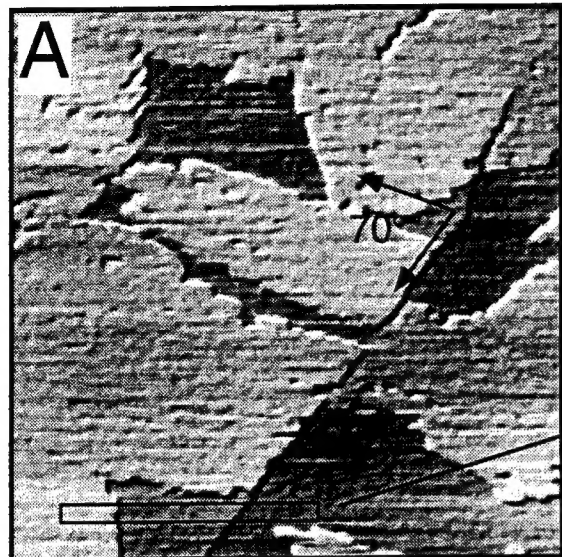
20 nm

A

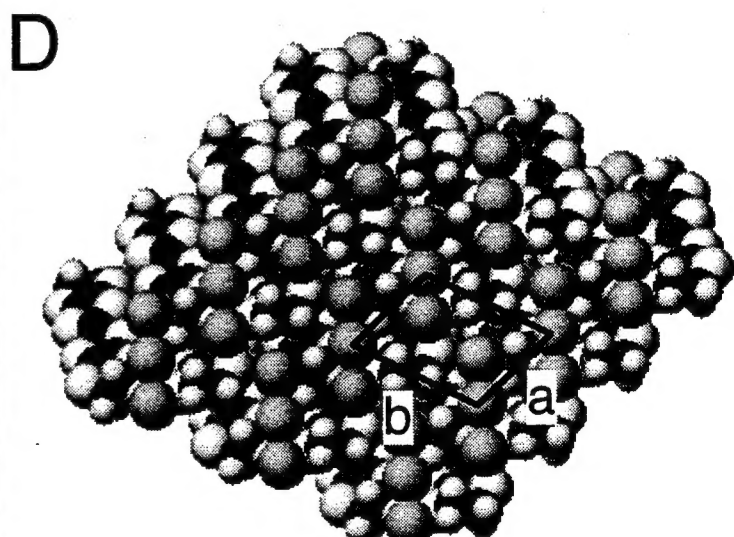
B

C

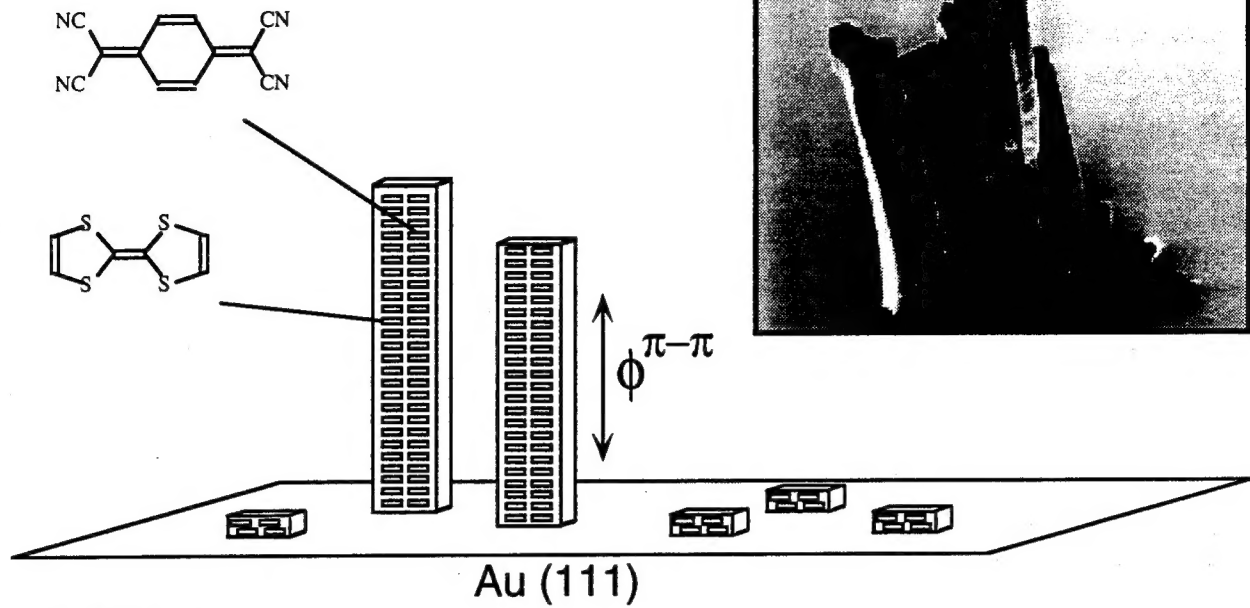




3 nm



## A $(\text{TTF})(\text{TCNQ})$



## B $\beta-(\text{ET})_2\text{I}_3$

